Order of operations for decoding superior colliculus activity for saccade generation

Husam A. Katnani and Neeraj J. Gandhi

You might find this additional info useful...

This article cites 48 articles, 23 of which can be accessed free at:
http://jn.physiology.org/content/106/3/1250.full.html#ref-list-1

Updated information and services including high resolution figures, can be found at:
http://jn.physiology.org/content/106/3/1250.full.html

Additional material and information about *Journal of Neurophysiology* can be found at:
http://www.the-aps.org/publications/jn

This infomation is current as of September 8, 2011.

Order of operations for decoding superior colliculus activity for saccade generation

Husam A. Katnani[1,4] and Neeraj J. Gandhi[1,2,3,4]

Departments of [1]Bioengineering, [2]Otolaryngology and [3]Neuroscience, [4]Center for Neural Basis of Cognition, University of Pittsburgh, Pittsburgh, Pennsylvania

Katnani HA, Gandhi NJ. Order of operations for decoding superior colliculus activity for saccade generation. *J Neurophysiol* 106: 1250–1259, 2011. First published June 15, 2011; doi:10.1152/jn.00265.2011.—To help understand the order of events that occurs when generating saccades, we simulated and tested two commonly stated decoding models that are believed to occur in the oculomotor system: vector averaging (VA) and center-of-mass. To generate accurate saccades, each model incorporates two required criteria: *1*) a decoding mechanism that deciphers a population response of the superior colliculus (SC) and *2*) an exponential transformation that converts the saccade vector into visual coordinates. The order of these two criteria is used differently within each model, yet the significance of the sequence has not been quantified. To distinguish between each decoding sequence and hence, to determine the order of events necessary to generate accurate saccades, we simulated the two models. Distinguishable predictions were obtained when two simultaneous motor commands are processed by each model. Experimental tests of the models were performed by observing the distribution of endpoints of saccades evoked by weighted, simultaneous microstimulation of two SC sites. The data were consistent with the predictions of the VA model, in which exponential transformation precedes the decoding computation.

sequence of decoding; dual microstimulation; vector averaging; vector summation; center-of-mass

THE SUPERIOR COLLICULUS (SC) is a critical, subcortical hub that plays a major role in converting sensory information into a motor command for saccade generation (Gandhi and Katnani 2011; Sparks 1986). Visual information in the SC is organized topographically in a logarithmic manner. A disproportionately large amount of SC tissue is allocated for (para-) foveal space and small-amplitude saccades, whereas a compressed region is attributed for the visual periphery and large-amplitude saccades (Cynader and Berman 1972; Robinson 1972). With the presentation of a stimulus, a population of neurons becomes active at a locus that represents the vector between the stimuli and line of sight (Wurtz and Goldberg 1972). Under ordinary circumstances, a comparable population discharges a high-frequency premotor burst to produce a saccade of the appropriate displacement (Sparks et al. 1976). To make certain that the saccadic eye movement lands near the desired location, two critical operations must be performed. One, the population response must be decoded using standard decoding mechanisms such as averaging or summation. Two, the SC output must undergo an exponential transformation to convert the saccade vector into visual coordinates (Ottes et al. 1986), the inverse transformation used to map visual space into SC

coordinates. Studies have implemented the order of these two operations in different fashions. To the best of our knowledge, no attempt has been made to distinguish the order of these operations.

In one scheme, the exponential transformation is applied to each SC neuron's location to represent it in vector coordinates (equivalently, visual space). A decoding mechanism is then applied to the transformed population output to yield saccade vector metrics (Fig. 1*A*). This study only considers the averaging decoding algorithm, and therefore, we will refer to this sequence as a vector-averaging computation (VA model). Research and computational models typically use this order of operations to decode saccade metrics (Van Opstal and Goossens 2008; Walton et al. 2005). In the other sequence, the decoding algorithm happens in collicular coordinates. It computes the optimal location of activity in units of millimeters using principles of center-of-mass (CM) or center-of-gravity. The optimal location then undergoes an exponential transformation to produce the saccade metric (CM model; Fig. 1*A*). Studies associated with averaging saccades (Arai et al. 1994; Glimcher and Sparks 1993) and the SC role in spatial feedback control (Anderson et al. 1998) have relied on this sequence to decode the saccade vector.

The primary objective of this study was to address the order in which the two operations are implemented. It should be emphasized that our focus is not to address the specific decoding algorithm. We recognize that vector summation (VS) is another prevalent algorithm used to decode SC activity (Goossens and Van Opstal 2006; Van Gisbergen et al. 1987). Previous modeling has demonstrated that VA and VS can generate approximately equivalent decoding predictions (Fig. 1*A*), despite accounting for two different decoding principles (Van Opstal and Van Gisbergen 1989). However, we concentrate on the comparison of VA and CM, due to their simple implementation and similar description of decoding that allows for a straightforward investigation pertaining to the order in which decoding and exponential transformation are implemented.

We first reconstructed and simulated the well-established VA and CM models that are often referred to or used to describe the sequences for decoding SC activity. Each was assessed by observing the response to a wide range of single target locations. Both produced nearly identical saccade endpoints (Fig. 1*B*), yielding no clear distinction between the two algorithms. When the models were tested for their predictions of decoding two simultaneous populations, as during an averaging saccade task, a large separation between endpoints was observed. Importantly, when the strength of each population
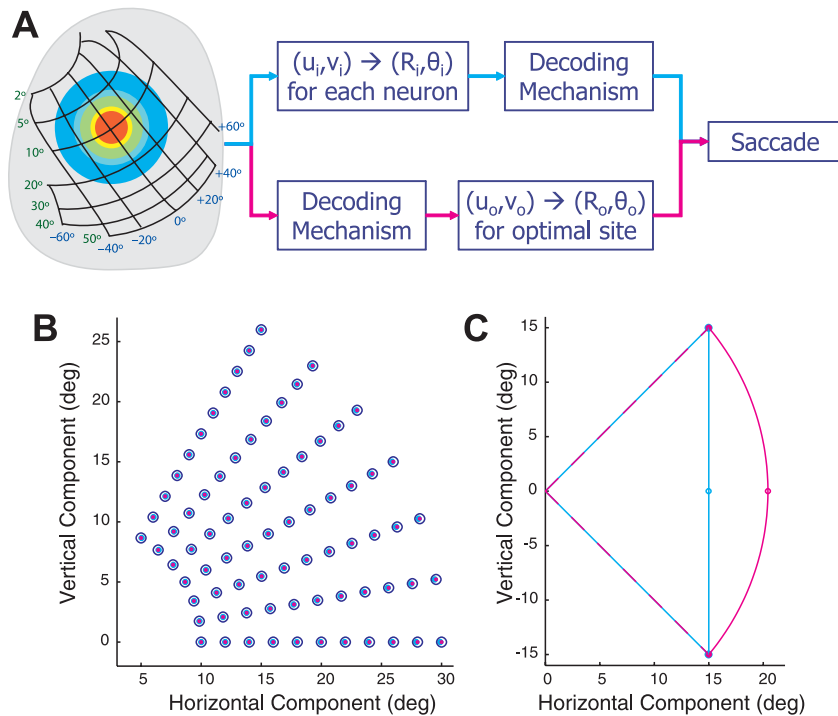
Fig. 1. Representation and predictions based on the order of decoding operations. *A*: order of operations for decoding population activity in the superior colliculus (SC) to generate saccades. The cyan path represents the sequence set by the vector averaging (VA) model. The SC coordinates of the neuron's (u_i, v_i) are first exponentially transformed into visual coordinates (R_i, Θ_i), and then a decoding mechanism is applied to the ensemble of neurons. The magenta path represents the sequence set by the center-of-mass (CM) model. The decoding mechanism determines the optimal location in SC coordinates (u_o, v_o), which then undergoes an exponential transformation to yield the saccade vector (R_o, Θ_o) in visual coordinates. *B*: saccade output (open magenta circles, CM output; cyan dots, VA output) of each path shown in *A* when tested with single target locations (open blue circles). *C*: saccade output of each path shown in *A* when tested with paired target locations $[(15°, 15°)$ and $(15°, -15°)]$. Dashed magenta and cyan lines represent saccade vector response to each target separately; open magenta and cyan circles represent the saccade endpoint of each model when decoding simultaneous populations of equal strength; solid magenta and cyan lines represent saccade endpoint distribution when decoding simultaneous populations of varying strengths.

was varied to simulate a wide range of weighted averaging saccade endpoints, the VA model predicted endpoint distributions along a straight line (Fig. 1*C*), whereas the CM model predicted distributions with curved geometry (Fig. 1*C*). Next, we experimentally tested the VA and CM models by examining saccade endpoint distributions elicited from simultaneous and weighted microstimulation of two SC sites. We focused on matching the geometry of the collected distributions to the predictions of each model. We found that nearly every distribution showed a straight geometry in the visual field, a result consistent with the predictions of the VA model.

A preliminary version of this study has been published previously (Gandhi and Katnani 2009).

MATERIALS AND METHODS

All procedures were approved by the Institutional Animal Care and Use Committee at the University of Pittsburgh and complied with the guidelines of the Public Health Service policy on Humane Care and Use of Laboratory Animals.

Subjects and Surgical Procedures

Three juvenile, male rhesus monkeys (*Macaca mulatta*) underwent one or more surgeries in a sterile environment and under isoflurane anesthesia. The initial procedure consisted of placing a Teflon-coated stainless steel wire (Baird Industries, Hohokus, NJ) under the conjunctiva of one eye and securing a head-restraint post to the skull. In the second procedure, one cylinder was cemented over a craniotomy. The chamber was placed stereotactically on the skull, slanted posteriorly at an angle of 38° in the sagittal plane. This approach allowed access to both colliculi and permitted electrode penetrations normal to the SC surface. After each surgery, the monkey was returned to its home cage and allowed to fully recover from surgery. Postoperatively, antibiotics and analgesics were administered as indicated in the protocol.

Experimental Procedures and Behavioral Tasks

Visual stimuli, behavioral control, and data acquisition were controlled by a custom-built program that uses LabVIEW architecture on a real-time operating system supported by National Instruments (Austin, TX) (Bryant and Gandhi 2005). Each animal was trained to sit in a primate chair with its head restrained, and a sipper tube was placed near the mouth for reward delivery. The animal was seated inside a dome surrounded by an alternating magnetic field, which induces a voltage in the eye coil and thus permits measurement of eye position (Robinson 1963). The animal fixates targets that were projected onto a circular mirror, which rear-reflects onto the isoluminant wall of the dome. Antiwarping software, obtained from Paul Bourke (University of Western Australia, Perth, Australia), allowed reflections from the mirror to appear undistorted and for distances to be properly transferred onto a curved surface. The monkey sat in the center of the dome, which has a radius of 1 m and spans ±150° horizontally and ±30° vertically of the visual field. A photodetector, positioned outside of the animal's field-of-view, detected the actual time of appearance of visual objects, which was then used to correct for time shifts induced by the projector's refresh rate.

In each experimental session, the animal performed the oculomotor gap task (discussed in next paragraph), as two platinum iridium microelectrodes (1.0–1.5 MΩ; MicroProbes for Life Science, Gaithersburg, MD)—each inserted into separate guide tubes, mounted on independent X–Y translation stages, and connected to different hydraulic microdrives (Narishige, Tokyo, Japan)—were individually advanced to the SC. The superficial layer of the SC was first identified by the presence of distinctive bursting of background activity associated with flashes of room lights. The electrode was then driven deeper into the SC until saccadic motor bursts were identified. At this stage, stimulation (40 μA, 400 Hz) was delivered during the gap period of the oculomotor task to determine the vector coordinates. The depth of the electrode was then minimally adjusted to obtain the shortest possible latency of the stimulation-evoked saccade (20–40 ms). Train duration was manually set (range: 100–300 ms) and always long enough to allow for completion of the stimulation-evoked movement. Suprathreshold stimulation parameters were chosen intentionally, as weaker settings often yielded nonoptimal saccades that exhibited

slower velocities and reduced amplitudes (Van Opstal et al. 1990), even with prolonged stimulation durations (Groh 2011; Guillaume and Pélisson 2001; Katnani and Gandhi 2010).

During data collection, the animal performed the oculomotor gap task. Each trial began with directing the line of sight to a fixation point for 300–500 ms before it is extinguished. Following a 200- to 400-ms "gap" interval, during which the animal was required to maintain the same eye position, another stimulus was illuminated in the visual periphery. Incorporation of the gap interval permits fixation to become disengaged prior to saccade preparation, allowing the oculomotor system to be more responsive to stimulation input. Stimulation was delivered during the gap period on a randomly selected 30% of the trials. For 20% of the trials, stimulation was delivered to each electrode individually, collecting site-specific saccade vectors; for 10% of the trials, stimulation was delivered simultaneously with no temporal shift between the pulses elicited from each electrode, producing a saccade whose amplitude and direction were influenced by the movement generated at each site independently. Stimulation onset occurred 100 ms after the offset of the fixation target, and if necessary, presentation of the peripheral stimulus was delayed until after stimulation offset. The animal was required to saccade to this target to earn a liquid reward. Depending on the vector elicited each day, the initial fixation target was controlled to ensure that the evoked movements were not reduced by orbital position effects.

Simultaneous stimulation first occurred with suprathreshold stimulation parameters matched at both electrodes (40 μA, 400 Hz, 100–300 ms). Distributions spanning a significant portion between the two single-site vectors were obtained by weighting the current intensity or frequency through one electrode in increments of 10 μA or 100 Hz while holding the parameters at the other electrode constant. After incrementing through a sufficient range, the stimulation parameters were once again matched, and the weighting was repeated for the second electrode.

Electrical Stimulation

Constant current stimulation trains were generated using a Grass S88X stimulator in combination with Grass PSIU6 isolation units. Trains consist of anodal phase-leading, biphasic pulses (0.25 ms). Frequency and current intensity were dictated by each experimental design, typically spanning in the range of 40–80 μA and 400–800 Hz.

Data Analyses

Each trial was digitized and stored for offline analysis. We used a combination of in-house software and Matlab 7.10.0 (R2010a). Horizontal and vertical eye position, along with onset and offset times of the stimulation train, was stored with a resolution of 1 ms. Component velocities were obtained by differentiating the eye-position signal. Onset and offset of stimulation-evoked saccades were then detected using a standard 30°/s velocity criteria, respectively.

Regression was used to best fit a straight line to the data and generate a coefficient of determination (R^2) to assess the goodness of fit. It is important to note that data sets that contain almost vertical or horizontal distributions yield R^2 values close to zero. This is a result of the regression analysis, which is not capable of estimating coefficients that can generate a line for distributions that have nearly constant dependent or independent variables. Therefore, the data were rotated to assess linearity. To verify that rotation did not affect our results, distributions were rotated systematically (in 5° increments), and a linear regression was applied for each rotation. This exercise revealed that R^2 values remained relatively invariant to rotation until the distribution reached a purely vertical or horizontal direction. The maximum R^2 value from each distribution was used in the analyses.

Computational Models

The VA and CM schemes are found in literature as computations and/or verbal descriptions used to explain how collicular activity is decoded for saccade generation (Anderson et al. 1998; Van Opstal and Goossens 2008). We reconstructed each model to test their fundamental properties with specific protocols that produce predictions that can be experimentally validated.

The right SC was modeled as a single layer grid of homogeneously distributed cells in millimeter coordinates (u, v). Each cell's vector components (H, V) were defined by exponentially transforming the collicular grid using the equations (Ottes et al. 1986)

$$H = A \cdot e^{\frac{u}{B_u}} \cdot \cos\left(\frac{v}{B_v}\right) - A \tag{1}$$

$$V = A \cdot e^{\frac{u}{B_u}} \cdot \sin\left(\frac{v}{B_v}\right) \tag{2}$$

with constant parameters $A = 3°$, $B_u = 1.4$ mm, and $B_v = 1.8$ mm.

A population of activity (P) was generated in the SC using a standard bivariate Gaussian equation

$$P = Fe^{\frac{-(u - u_o)^2 + (v - v_o)^2}{2\sigma^2}} \tag{3}$$

The strength and variance ($F = 500$ spikes/s and $\sigma = .5$ mm) of the population were set by the values reported in Van Gisbergen et al. (1987). Outside a radius of 2σ, population activity was set to zero. The population was centered at cells (u_o, v_o), calculated using the horizontal (H_t) and vertical (V_t) component of the desired or input target location (Optican 1995; Ottes et al. 1986)

$$u_o = \frac{B_u}{2} \cdot \log\frac{(H_t + A)^2 + V_t^2}{A^2} \tag{4}$$

$$v_o = B_v \cdot \tan^{-1}\left(\frac{V_t}{H_t + A}\right) \tag{5}$$

By repeating *Eqs. 3–5*, another target location could also be incorporated to generate a second, simultaneously active population in the SC. In cases where a portion of each population shared millimeter coordinates, the overlapping activity was summed. If overlapping activity were averaged, as opposed to summed, we found minute differences in the decoded saccade vector (less than one-tenth of a degree). Furthermore, neural recordings in the SC have demonstrated that the presence of competing populations can reduce the overall SC activity (Basso and Wurtz 1997; Li and Basso 2005); therefore, we also reduced the firing rate of our overall simulated activity profiles by 40%, in accordance with observations from neural recordings during saccades directed to two targets presented simultaneously (Edelman and Keller 1998). To avoid border effects, all target locations (single or paired) were restricted to visual space that would generate populations completely confined within the SC. Generated populations were then decoded through two different algorithms.

CM computation. Equation 6 performs an average in uniform millimeter space to find the center of the population that delineates the optimal saccade vector [r_n is the mean firing rate of cell n, and C_n denotes the spatial location (u, v) of each active cell in millimeters].

$$CM(u_o, v_o) = \frac{\sum_{n=1}^{N} r_n \cdot C_n}{\sum_{n=1}^{N} r_n} \tag{6}$$

The resulting coordinates (u_o, v_o), calculated from the equation, were then exponentially transformed (*Eqs. 1* and *2*) to obtain the saccade vector in visual coordinates.

VA computation. Equation 7 first involves exponentially transforming all active cells (*Eqs. 1* and *2*) to derive R_n, the vector components (H, V) encoded by active cell n.

$$VA(H, V) = \frac{\sum_{n=1}^{N} r_n \cdot \eta \cdot R_n}{\sum_{n=1}^{N} r_n} \qquad (7)$$

The weighted VA of all contributions was then calculated to obtain the saccade vector in visual coordinates (Lee et al. 1988; Van Opstal and Goossens 2008).

In addition to weighing each vector contribution with mean firing rate, a fixed scaling constant, η, was required. We found that the model yielded accurate responses to a target location (12°,12°) if η had a value of 0.9768. Once determined, η was fixed for all target locations.

Weighing procedure. As observed in *Eqs. 6* and *7*, each averaging computation involves a weight defined by the mean firing rate of each cell. In cases where paired target locations were input to each model, the mean firing rate could be manipulated by creating Gaussians with different population strengths. This was accomplished by increasing the strength (F_1) of one population while holding the strength (F_2) of the second population constant

$$F_1 = w + F, F_2 = F \qquad (8)$$

where w is an allotted increment of spikes/s. *Equation 8* is then repeated, where F_2 is varied, whereas F_1 is held constant. A procedure of this manner allows for the models to simulate a wide range of weighted averaging saccades between the input target locations.

RESULTS

Model Response to Single and Paired Target Locations

Each computational model was simulated with a wide range of single target locations in the first quadrant. The results of the simulations are shown in Fig. 1*B*. Both models are shown to respond to each target location with high accuracy [CM, mean endpoint error 0.0019° (SD: 0.001); VA, mean endpoint error 0.0342° (SD: 0.0273)]. Thus the saccade endpoints generated from single target locations do not distinguish between the two mechanisms.

Each computation was then performed using two simultaneous target locations. The example shown in Fig. 1*C* illustrates the predictions for the target pairs [(15°,15°) and (15°,−15°)]. The VA and CM endpoint prediction when decoding two simultaneous populations of equal strength are shown to be separated by 5.45°. Next, the strength of each population was varied (see MATERIALS AND METHODS, *Computational models*) to generate a distribution of weighted vector predictions between the target locations. As observed in Fig. 1*C*, the separation between predictions varies due to each model outputting distributions of different geometries. The VA generated a straight distribution, whereas the CM generated a curved distribution. The straight vs. curved predictions were consistent across all input target pairs with the requirement of different directions.

Analysis of Stimulation-Induced Distributions

A total of 26 stimulation-induced vector pairs (Fig. 2) was studied from three monkeys, sampling a portion of the SC vector map that spanned from ~2° to 40° in amplitude and ~−70° to 70° in direction. Collectively, the vector pairs exhibited amplitude differences anywhere between 0° and 30° and directional differences between 25° and 105°. The distribution of endpoints was investigated by systematically varying current intensity (14 sites), frequency (5 sites), or both (7 sites; frequency was held constant, whereas current was varied and
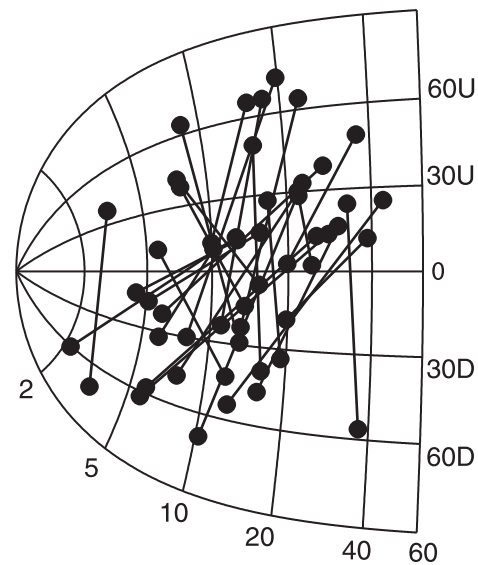

Fig. 2. Distribution of paired stimulation sites. The vector evoked by each site is shown by a black dot, and the pair is connected by a line. All 26 paired sites are represented on the SC saccade motor map. Numbers spanning from left to right indicate saccade amplitude. Vertically aligned text (*right*) denotes saccade direction. U, up; D, down.

vice versa), producing a total of 33 pairs for analysis. Two vector pair examples are shown in Fig. 3, *A* and *B*. The distribution of saccade endpoints was obtained by varying current intensity (Fig. 3*A*) and frequency (Fig. 3*B*). We found that varying either parameter produced comparable distributions; therefore, all distributions generated by varying current intensity or frequency were analyzed for the purposes of this investigation. Superimposed on top of the collected data are the VA and CM predictions, simulated with the corresponding vector pairs (cyan and magenta lines, respectively).

Figure 3, *C* and *D*, illustrates the logarithmic transformation (*Eqs. 4* and *5*) of each collected endpoint into SC coordinates. By performing this transformation, we observe the center of each active population in the SC that would generate such endpoints. For comparison, the geometry of the computed population centers, decoded by the CM model when simulated with the corresponding vector pair, is also shown in the figure. Note that when the strength of each population is varied within the CM model, the decoded population center shifts on a straight line between the two SC coordinates set by the input vector pair. Thus the VA and CM models generate predictions on a straight line (Fig. 3, *A–D*) in different domains (visual vs. SC coordinates). To assess which decoding mechanism is more likely the candidate to produce the observed data, we performed a linear regression (see MATERIALS AND METHODS, *Data analyses*) on the endpoint distribution in visual space (e.g., Fig. 3*A*) and on the same distribution transformed into SC coordinates (e.g., Fig. 3*C*). Figure 4 illustrates the comparison of R^2 values in each domain across all collected vector pairs. Almost all values lie above unity, indicating a significantly (*t*-test; $P = 3.04e^{-4}$) better representation of linearity in visual space. The significance of the result suggests that averaging occurs within visual coordinates, as almost all distributions had strong linear fits in visual space. Although a large portion of values also demonstrates good linear fits in SC coordinates, this does not detract from the fact that the geometry of the collected end-

Fig. 3. Family of saccades evoked by weighted, simultaneous stimulation of 2 SC sites. *A* and *B*: red and green trajectories represent stimulation of each site separately; blue, orange, yellow, magenta, and black trajectories and endpoints correspond to the saccades generated by paired stimulation of different current intensities in *A* and frequencies in *B* (see *key* for stimulation parameter values); solid cyan and magenta lines represent VA and CM predictions, respectively, when simulated with the corresponding vector pair. *Key*: if the stimulation parameter of *Site 1* is being varied (*left column*), the stimulation parameters at *Site 2* are fixed (*right column*); this procedure is then repeated for *Site 2*. As a result, there is a reflection of repeated colors for the elicited saccade vectors when 1 site is weighed over the other. *C* and *D*: transformation of endpoint distributions into SC coordinates (open blue circle); solid magenta line represents the SC coordinates decoded in the CM model when simulated with the corresponding vector pair.
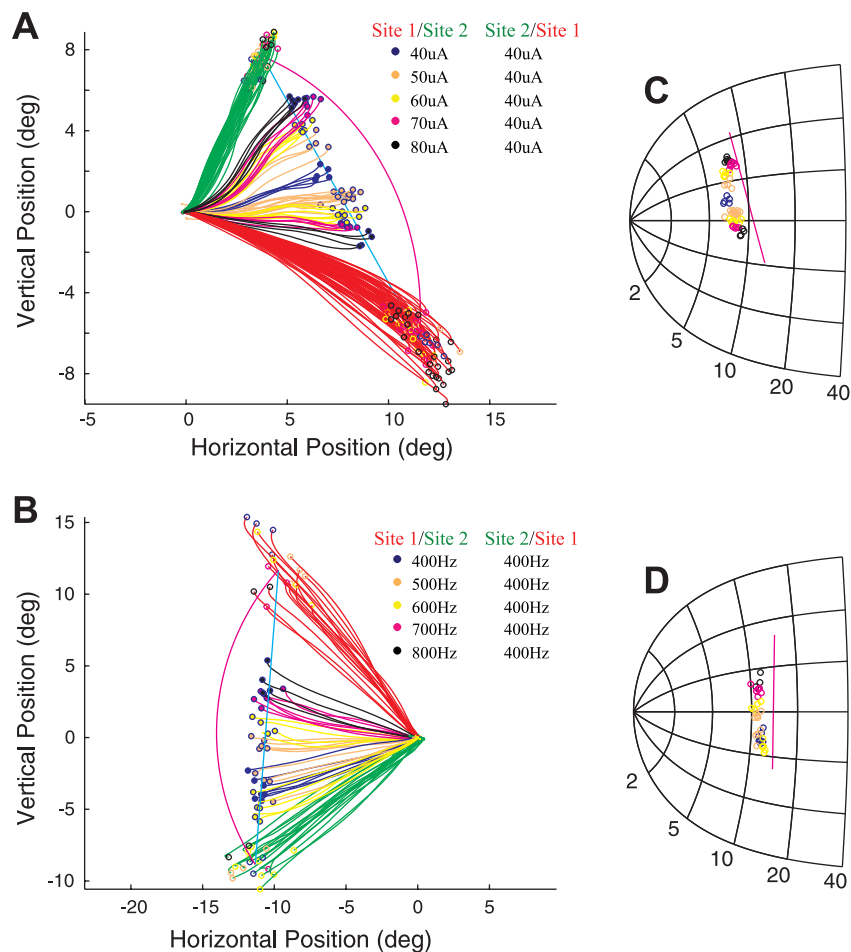
point distributions showed little to no curvature in visual space (as would be predicted by a CM model).

Visual assessment of the data in SC coordinates indicated the presence of curvature even for distributions with high R^2 values from the linear regression analysis. For example, the regression on the distribution shown in Fig. 5*A* resulted in a R^2
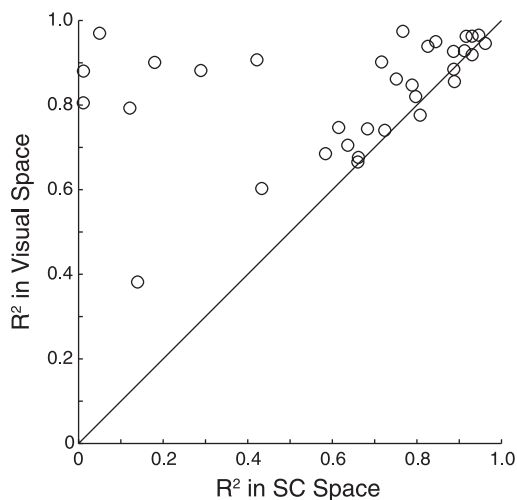

Fig. 4. Comparison of endpoint distributions in visual and SC coordinates. Coefficient of determination (R^2) values (open circles), derived from linear regressions performed on saccade endpoint distributions in visual space (*y*-axis) and when transformed into SC coordinates (*x*-axis). Solid line represents unity line.

value of 0.9124; however, one can clearly observe curvature in the data. Therefore, we developed an index of curvature (IC) analysis to quantify any curvature within the distributions in visual space and when transformed into SC coordinates. The analysis involves performing a two-dimensional average on the distribution of points to obtain a description of its geometry (Fig. 5*A*). Points along the geometric fit were then projected onto a straight line that connected the ends of the overall distribution. The curvature of the data was then quantified by selecting the projection of maximum magnitude and dividing it by the magnitude of the line connecting the overall ends of the distribution. A noteworthy piece of information is that the two-dimensional average did not generate perfect geometry descriptions due to noise in the data. Thus distributions that show no curvature still generated nonzero IC values due to the geometric fit not perfectly overlapping with the straight line that connects the ends of the distribution. To ensure that projections signified actual deviation from straight geometries and were not just a result of noise in the data, all selected magnitudes were classified according to the variance of the data. Magnitudes that did not exceed at least one SD from the two-dimensional average fit were classified as insignificant. The amount of curvature recorded from each distribution when in visual space vs. SC coordinates is shown in Fig. 5*B*. Almost all values lie below the unity line demonstrating that a significant (*t*-test; $P = 2.13e^{-10}$) amount of curvature is introduced into the distribution when transformed into SC coordinates. Furthermore,
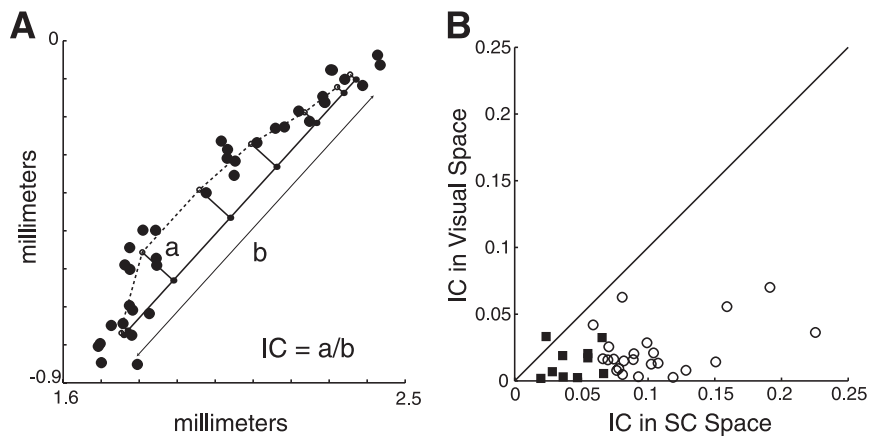
Fig. 5. Comparison of index of curvature (IC) values in visual and SC coordinates. *A*: example of IC derivation on transformed endpoint distribution (large black dots) in SC coordinates. Dashed line represents geometry fit; solid line (*b*) represents a straight path between the overall ends of the distribution; small open circles with connecting lines represent projections from the geometry fit to the straight path. The IC value is computed as the maximum projection length (*a*) divided by *line b*. *B*: IC values derived from analysis on saccade endpoint distributions in visual space (*y*-axis) and when transformed into SC coordinates (*x*-axis). Solid line represents unity line; solid squares represent insignificant IC values in both visual and SC coordinates; open circles represent significant IC values in SC coordinates and insignificant IC values in visual coordinates.

all values are insignificant in visual coordinates, reinforcing that distributions in the visual field are relatively straight. A result of this manner contradicts the predictions of the CM model.

DISCUSSION

Early studies revealed that the SC contains a logarithmically distributed map in visual coordinates, a result that requires its motor commands to be exponentially transformed for saccade vectors to conform to visual space (Sparks 1986). The nature of this conversion causes the output of an averaging scheme to become dependent on whether its computation occurs before or after the exponential transformation. VA and CM mechanisms, therefore, carry different interpretations for decoding eye movements. We stress this difference due to the observation that an averaging computation is often considered an acceptable decoding method, yet statements of this manner are generally qualitative and noncommittal on the implementation strategy (e.g., Sooksawate et al. 2011). Although there is a significantly different result to each sequence, the two schemes are commonly classified under the umbrella of population VA. We simulated both VA and CM models with two simultaneous populations of activities and found that they predict different saccade endpoint distributions. Specifically, differentially weighing the two populations produces endpoint distributions that reside on a straight line in the VA model but conform to a curved geometry in the CM model (Fig. 1*C*). These predictions were tested by examining the distribution of weighted averaging saccade endpoints through simultaneous stimulation of two sites in the SC. Regression of the data revealed good linear fits in the visual field, as predicted by the VA decoding sequence. Furthermore, when endpoint distributions were log transformed into SC coordinates, we found that the millimeter coordinates calculated by the CM model did not align well with the coordinates of the transformed data. Therefore, we conclude that our results favor the networked sequence of decoding that is implicit to the VA model.

Neural Implementation of Decoding Mechanisms

Implementation of both VA and CM mechanisms requires two steps: decoding population activity using a normalization (averaging)-based algorithm and an exponential transformation to align movements in visual coordinates. Although physiological and theoretical evidence for normalization has been provided in various systems, such as visual cortex of primates

(Carandini and Heeger 1994) and olfactory processing in the locust (Papadopoulou et al. 2011), a neural correlate in the saccadic system has been elusive. A VS algorithm that does not require normalization has been proposed as an alternate mechanism for decoding SC activity (Goossens and Van Opstal 2006; Van Gisbergen et al. 1987); this mechanism is discussed in the last paragraph of this section.

Projections from the SC to the burst generator are weighted according to the site of origin (Moschovakis et al. 1998). Specifically, the efficacy of the projections increases for neurons originating from regions encoding increasingly larger amplitude vectors. This trend in projection weights conforms to the transformation needed to convert saccade commands into visual coordinates and, at least qualitatively, is consistent with the requirements of the VA mechanism. However, it should be noted that the monotonic increase in weight is not equivalent to the exponential relationship required of the VA algorithm.

Neural implementation of the CM mechanism is potentially more complicated and is not explicitly supported by our data. Nevertheless, we speculate on potential schemes. Let us first consider decoding saccade metrics from a single active region in the SC, such as activation resulting from a single target. The reconstruction of a population response from neural recordings in the SC has demonstrated that activity is well represented by a static Gaussian mound that rises and falls (Anderson et al. 1998). In this manner, the cells at the center of the active population will have the highest firing rate and the longest burst duration. Therefore, one such implementation may be that the center cells are the only significant representation of the intended saccade vector (Van Opstal and Kappen 1993). Another pivotal feature is that because CM decoding occurs before the exponential transformation, another explicit transformation would be needed to properly generate saccades in the visual field. Such an operation could be performed in the cerebellum and/or the nucleus reticularis tegmenti pontis, to which the SC projects heavily (Harting 1977; Huerta and Harting 1984; Scudder et al. 1996) and whose functional role in processing SC activity is still unclear.

The CM mechanism is most prominent, not as the primary saccadic decoding mechanism but rather, when implemented prior to population decoding to explain a neural correlate for the generation of regular latency-averaging saccades (Arai et al. 1994; Glimcher and Sparks 1993). Presiding through the use of lateral interactions, a CM correlate occurs when a mass

distribution of activity, resulting from multiple visual stimuli, can form a single population at an intermediate location in the SC. The single population can then be deciphered through a different mechanism (e.g., VA and VS). Nevertheless, we demonstrate in this investigation that implementing a process of this nature generates nonintuitive results (see *Relation to averaging saccade mechanisms* below). It seems more reasonable to speculate that lateral interactions in the SC manipulate the spatial and temporal register of activity to form broad population profiles (Edelman and Keller 1998), which allows for the incorporation of information from the visual stimuli. Therefore, one must be cautious when describing and/or using an averaging scheme to explain saccade generation, as the implementation is important for appropriately characterizing decoding properties in the oculomotor system.
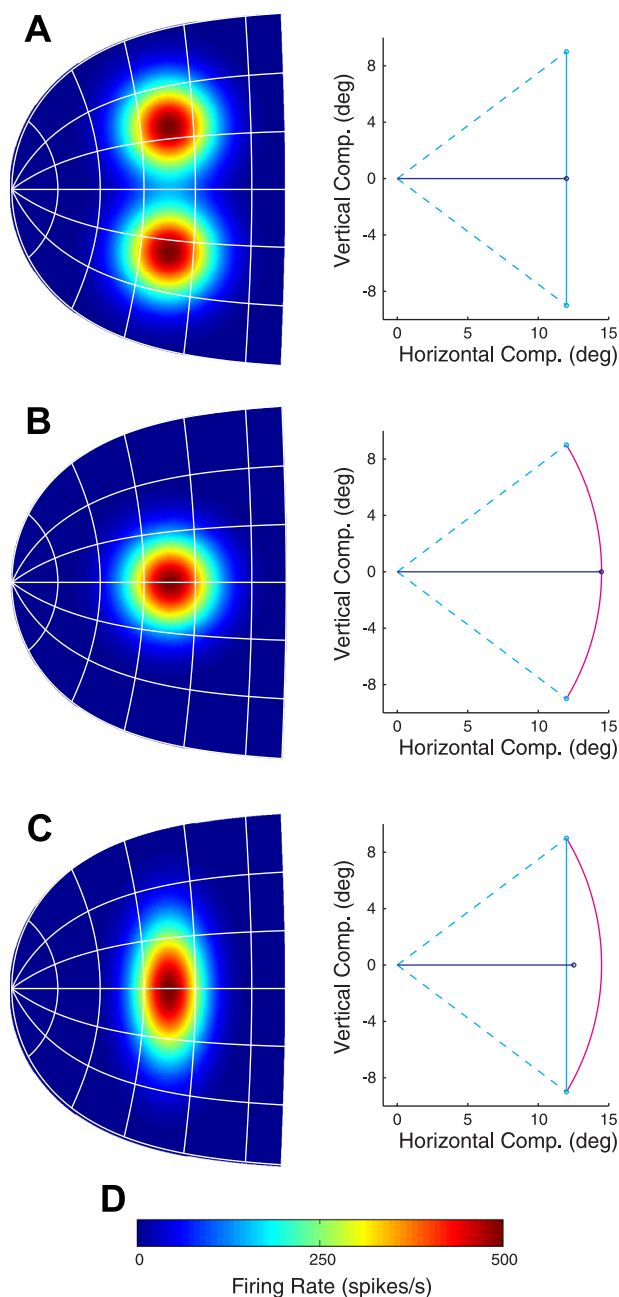
A VS model could also be a plausible candidate to contrast with the CM model. This computation also assumes a sequence in which the decoding operation occurs after the neural activity has been exponentially transformed but stipulates that the weighted vector contribution of each neuron in the active population is summed and not normalized (Goossens and Van Opstal 2006; Van Gisbergen et al. 1987). Furthermore, when the computation incorporates spatial interactions in the SC, the model can predict stimulation-induced activity patterns and produce saccade vector predictions that align with the VA model (Van Opstal and Van Gisbergen 1989). Interestingly, the model's predicted discharge patterns correspond nicely with the neural activity correlated to express latency-averaging saccades. Therefore, the neural mechanism described by a VS model could also be a likely candidate to explain decoding SC activity and does not alter the finding that decoding occurs after exponential transformation. We chose to limit our focus on the VA model due to its loose interpretation with the CM model.

Relation to Averaging Saccade Mechanisms

Edelman and Keller's (1998) examination of averaging saccades of express latencies in a two-target task revealed that activity in the deeper layers of the SC best matches the profile of two simultaneous populations corresponding to the two visual targets. Therefore, the discharge of neurons was centered at loci corresponding to the paired target locations and not the site encoding the elicited saccade vector. Their finding exemplifies the reflexive nature of the task, which allows visual activity to be immediately pipelined to the motor layers (Dorris et al. 1997). We simulated these findings (Fig. 6A) to distinguish between the VA and CM mechanisms and found results that conform to the predictions of the VA hypothesis.

Averaging saccades can also be generated at regular (nonexpress) reaction times. How is activity distributed across SC neurons for this subset of movements? Glimcher and Sparks (1993) suggested that the initial visual activity, dependent on target configuration, is processed to generate a single population centered at an intermediate location. To simulate this finding, a target pair location was chosen, and *Eq. 6* was first used to determine an intermediate coordinate location (u_o, v_o)

Fig. 6. Simulations of the VA model to account for the generation of averaging saccades. *A, left*: 2 equal-strength populations of active neurons positioned at sites encoded by chosen target pair locations [(12°,12°) and (12°,−12°)]. *Right*: solid (horizontal) blue line represents the saccade vector prediction generated by the VA model when decoding the simultaneous activity distributions. Dashed cyan lines represent single-site vector prediction generated when each population is decoded separately. Solid (vertical) cyan line represents the geometry of the VA model predicted by differentially weighing the 2 populations. *B, left*: single population of activity formed at an intermediate location between the 2 populations shown in *A* (see DISCUSSION, *Relation to averaging saccade mechanisms*). The width of this population is identical to those used for saccades directed to a single target. *Right*: solid (horizontal) blue line represents the VA saccade output when decoding this population activity. Solid magenta line represents the geometry of the endpoints generated by the VA model, as the spatial center of the population shifts from 1 target location to the other. *C, left*: population activity centered at an intermediate location between the populations shown in *A* but with broad directional spread. The 2-dimensional variance of this population is conceptual and was manually set to simulate the broad activity profiles reported in Edelman and Keller (1998). *Right*: solid (horizontal) blue line represents saccade output from the VA model when decoding this activity. Note that its endpoint falls much closer to the output predicted by averaging vectors in visual space (cyan trace). *D*: color scale represents the firing rate (spikes/s) of population activity shown in the *left columns*.

between the two simultaneous populations generated from the input target pair. Next, *Eq. 3* was used to generate a single population at the calculated coordinates (u_o, v_o). Finally, the VA computation, as stated in MATERIALS AND METHODS, was used to decode the single population and output a saccade vector. Interestingly, we found that simulations of our model generated saccade vectors that overshot a VA in visual coordinates (Fig. 6*B*). Furthermore, when the strength of each population was varied incrementally, we discovered that the model predicted endpoints that lie on the curved geometries, which matched those of the CM model. This result is a consequence of the required CM decoding needed to calculate the intermediate location of the single population. Research and computational models that use the CM mechanism to explain and simulate averaging saccades will generate vectors that overshoot the expected weighted average (Arai et al. 1994). The hypermetric movements simulated by this architecture do not conform to experimental findings. Other studies have reported that SC activity during regular latency-averaging saccades exhibits a representation that is intermediate between two target-activated populations and a single saccade-related ensemble (Edelman and Keller 1998; Van Opstal and Van Gisbergen 1990). We simulated the VA model (Fig. 6*C*) with the incorporation of widespread SC activity [the population profile was manually altered to mimic the findings discussed in Edelman and Keller (1998) and Van Opstal and Van Gisbergen (1990)] and found that the VA model indeed produces vector predictions closer to observed averaging saccades. This would imply that although averaging saccades of regular reaction times do not exactly match the profile of two simultaneous populations, the activity remains broad enough to incorporate sufficient information from the target configuration, allowing the decoding mechanism to generate saccades that land near or in between the visual stimuli.

Averaging saccades of express and regular latencies not only differ in their spatial distribution of activity but also have been shown to have different dynamics, where the firing rates at express latencies are much lower (Edelman and Keller 1998). We simulated whether a reduction in SC activity would affect our model predictions. Accordingly, we reduced the output firing-rate patterns of each model by 40%. The averaging saccade predictions from the VA and CM models were similar for the attenuated and intact activity profiles (not shown). We anticipated this conclusion, as both models derive the metrics of saccades with an averaging formula that relies on the spatial distribution of activity and not the level of activity. We recognize that such a method is probably too simplistic to describe neural mechanisms; however, the crude approximation of an averaging scheme does resemble the data, allowing for a sufficient investigation of decoding sequence. Furthermore, we cannot assume that suprathreshold stimulation induces low levels of neural activity, such as during averaging saccades at express latencies; yet, stimulation still elicits averaging saccade endpoints that qualitatively match naturally evoked averaging saccades. Van Opstal and Van Gisbergen (1989) proposed a potential method for predicting patterns of dual stimulation activity; however, the paper focused only on current-distance activation. Additional research is needed to determine how a large range of both current intensity and frequency stimulation induces neural activity in the SC.

Interpretation of Stimulation Results

The use of suprathreshold stimulation parameters likely drives SC neurons at a high frequency and corrupts the time-scale necessary for networked neurons to interact. Therefore, our experimental technique for generating distributions of weighted averaging saccade endpoints may bypass the network necessary to observe the results of a CM mechanism. Nevertheless, under the assumption that stimulation only activates the output of the SC, our data still imply that there is a system that is fully capable of producing weighted averaging movements (i.e., transformation before decoding), regardless of the brute force stimulation technique. The weighted projections from the SC to the burst generator (see DISCUSSION, *Neural implementation of decoding mechanisms*, above) (Moschovakis et al. 1998) suggest that the transformation occurs downstream of the SC. However, it is important to recognize that ascending outputs of the SC could also contribute to the transformation. For example, stimulation of the deep layers could activate neurons in the superficial layers (Isa and Hall 2009; Vokoun et al. 2010), which in turn could recruit the intraparietal cortex via the pulvinar (Clower et al. 2001). Neurons in the deep SC layers could also recruit the frontal eye fields (FEFs) via the mediodorsal thalamus (Sommer and Wurtz 2004). In addition, these and other oculomotor areas with direct projections to the SC could be activated antidromically. We speculate that structures activated through the ascending output are not likely to exert a role in producing SC stimulation-evoked saccades, because their inactivation does not produce deficits in mediating motoric control (Sommer and Wurtz 2002; Wilke et al. 2010). Furthermore, the primary FEF output pathway involved in saccade generation is likely relayed through the SC (Hanes and Wurtz 2001), and the same could be true for other cortical regions. These results collectively imply that saccades evoked by SC stimulation are primarily mediated through descending outputs to the brain stem.

We must assume that current intensity primarily influences the spatial extent of activation, and frequency mainly controls the temporal features of activity (McIlwain 1982; Ranck 1975; Tehovnik 1996; Vokoun et al. 2010). From an experimental perspective, our data demonstrate that current intensity vs. frequency generates comparable averaging saccade distributions. We speculate that this result could be due to using stimulation parameters in the suprathreshold range, where spatial and temporal integration mechanisms may become functionally equivalent. Another possible explanation could arise from the intrinsic properties of the SC, which could shape stimulation-induced activity to maintain features of naturally generated discharge patterns. Further investigation is needed to elucidate how stimulation evokes activity in the SC (Katnani and Gandhi 2010). From a modeling perspective, our simulations vary population strength by changing the firing rate or level of activity, thus aligning with the assumptions behind how stimulation frequency induces activity. To observe the effects of current intensity, we also simulated each model by varying the width (σ) of the population as opposed to the firing rate. We found that the saccade vector predictions of the CM model only significantly changed with population widths that generated drastic border effects ($\sigma > 1.5$ mm). In contrast, the VA predictions changed well before border effects, due to the nonlinear nature of the SC saccade vector map. To resolve such

an issue, the model's scaling constant (see MATERIALS AND METHODS, *VA computation*) must change along with the population width. Nevertheless, regardless of any change in the derived saccade vectors, the geometry of the predicted saccade distributions from each model always remained the same. This is an important result, as the focus of this study is not to distinguish the properties of decoding mechanisms in the SC but to probe the order of operations that occurs during saccade generation.

Lastly, we cannot assume that dual microstimulation induces patterns of activity in the SC, which matches visually evoked activity; however, since our stimulation-induced endpoint distributions qualitatively match visually guided, averaging saccade endpoint distributions (Chou et al. 1999; Edelman and Keller 1998; Glimcher and Sparks 1993; Van Opstal and Van Gisbergen 1990), it seems reasonable to assume that the order of operations that occurs (exponential transformation then decoding), whether driven by stimulation or visual targets, is similar.

Previous Studies Using Dual Microstimulation in the Oculomotor System

Assessment of VA in the oculomotor system through dual microstimulation is limited. Dual microstimulation studies in the 1960s and 1970s (Robinson 1972; Robinson and Fuchs 1969; Schiller et al. 1979) were typically subexperiments, resulting in a qualitative assessment of the elicited saccades and nothing more than a single illustration. In fact, stimulation-induced VA in the SC has only been reported briefly in one investigation of the colliculus (see Fig. 5 in Robinson 1972), where weighted VA was not quantified, and no alternate mechanisms to account for the observed saccade patterns were considered. Recent dual microstimulation experiments in the oculomotor system have employed temporal shifts between the stimulation trains elicited at each electrode. Noto and Gnadt (2009) evaluated the generation of curved saccades, whereas Brecht et al. (2004) attempted to differentiate between VA and VS. Our analysis of endpoint distributions provides a systematic and in-depth analysis of the long-standing but poorly tested weighted VA hypothesis, which is necessary to link averaging saccades across literature in the oculomotor field.

DISCLOSURES

No conflicts of interest, financial or otherwise, are declared by the author(s).

REFERENCES

Anderson RW, Keller EL, Gandhi NJ, Das S. Two dimensional saccade-related population activity in superior colliculus in monkey. *J Neurophysiol* 80: 798–817, 1998.

Arai K, Keller EL, Edelman JA. Two-dimensional neural network model of the primate saccadic system. *Neural Net* 7: 1115–1135, 1994.

Basso MA, Wurtz RH. Modulation of neuronal activity by target uncertainty. *Nature* 389: 66–69, 1997.

Brecht M, Singer W, Engel AK. Amplitude and direction of saccadic eye movements depend on the synchronicity of collicular population activity. *J Neurophysiol* 92: 424–432, 2004.

Bryant CL, Gandhi NJ. Real-time data acquisition and control system for the measurement of motor and neural data. *J Neurosci Methods* 142: 193–200, 2005.

Carandini M, Heeger DJ. Summation and division by neurons in primate visual cortex. *Science* 264: 1333–1336, 1994.

Chou IH, Sommer MA, Schiller PH. Express averaging saccades in monkeys. *Vision Res* 39: 4200–4216, 1999.

Clower DM, West RA, Lynch JC, Strick PL. The inferior parietal lobule is the target of output from the superior colliculus, hippocampus, and cerebellum. *J Neurosci* 21: 6283–6291, 2001.

Cynader M, Berman N. Receptive-field organization of monkey superior colliculus. *J Neurophysiol* 35: 187–201, 1972.

Dorris MC, Paré M, Munoz DP. Neuronal activity in monkey superior colliculus related to the initiation of saccadic eye movements. *J Neurosci* 17: 8566–8579, 1997.

Edelman JA, Keller EL. Dependence on target configuration of express saccade-related activity in the primate superior colliculus. *J Neurophysiol* 80: 1407–1426, 1998.

Gandhi NJ, Katnani HA. Motor functions of the superior colliculus. *Annu Rev Neurosci* 34: 203–229, 2011.

Gandhi NJ, Katnani HA. Single and dual microstimulation in the superior colliculus: effects of stimulation intensity and frequency. *Soc Neurosci Abstr*, Program No. 851.7, 2009.

Glimcher PW, Sparks DL. Representation of averaging saccades in the superior colliculus of the monkey. *Exp Brain Res* 95: 429–435, 1993.

Goossens HH, Van Opstal AJ. Dynamic ensemble coding of saccades in the monkey superior colliculus. *J Neurophysiol* 95: 2326–2341, 2006.

Groh JM. Effects of initial eye position on saccades evoked by microstimulation in the primate superior colliculus: implications for models of the SC read-out process. *Front Integr Neurosci* 4, 2011.

Guillaume A, Pélisson D. Gaze shifts evoked by electrical stimulation of the superior colliculus in the head-unrestrained cat. I. Effect of the locus and of the parameters of stimulation. *Eur J Neurosci* 14: 1331–1344, 2001.

Hanes DP, Wurtz RH. Interaction of the frontal eye field and superior colliculus for saccade generation. *J Neurophysiol* 85: 804–815, 2001.

Harting JK. Descending pathways from the superior collicullus: an autoradiographic analysis in the rhesus monkey (*Macaca mulatta*). *J Comp Neurol* 173: 583–612, 1977.

Huerta MF, Harting JK. The mammalian superior colliculus: studies of its morphology and connections. In: *Comparative Neurology of the Optic Tectum*, edited by Vanegas H. New York: Plenum, 1984, p. 687–773.

Isa T, Hall WC. Exploring the superior colliculus in vitro. *J Neurophysiol* 102: 2581–2593, 2009.

Katnani HA, Gandhi NJ. Analysis of current and frequency stimulation permutations in the superior colliculus. *Soc Neurosci Abstr*, Program No. 77.9, 2010.

Lee C, Rohrer WH, Sparks DL. Population coding of saccadic eye movements by neurons in the superior colliculus. *Nature* 332: 357–360, 1988.

Li X, Basso MA. Competitive stimulus interactions within single response fields of superior colliculus neurons. *J Neurosci* 25: 11357–11373, 2005.

McIlwain JT. Lateral spread of neural excitation during microstimulation in intermediate gray layer of cat's superior colliculus. *J Neurophysiol* 47: 167–178, 1982.

Moschovakis AK, Kitama T, Dalezios Y, Petit J, Brandi AM, Grantyn AA. An anatomical substrate for the spatiotemporal transformation. *J Neurosci* 18: 10219–10229, 1998.

Noto CT, Gnadt JW. Saccade trajectories evoked by sequential and colliding stimulation of the monkey superior colliculus. *Brain Res* 1295: 99–118, 2009.

Optican LM. A field theory of saccade generation: temporal-to-spatial transform in the superior colliculus. *Vision Res* 35: 3313–3320, 1995.

Ottes FP, Van Gisbergen JA, Eggermont JJ. Visuomotor fields of the superior colliculus: a quantitative model. *Vision Res* 26: 857–873, 1986.

Papadopoulou M, Cassenaer S, Nowotny T, Laurent G. Normalization for sparse encoding of odors by a wide-field interneuron. *Science* 332: 721–725, 2011.

Ranck JB Jr. Which elements are excited in electrical stimulation of mammalian central nervous system: a review. *Brain Res* 98: 417–440, 1975.

Robinson DA. A method for measuring eye movement using a scleral search coil in a magnetic field. *IEEE Trans Biomed Eng* 10: 137–145, 1963.

Robinson DA. Eye movements evoked by collicular stimulation in the alert monkey. *Vision Res* 12: 1795–1808, 1972.

Robinson DA, Fuchs AF. Eye movements evoked by stimulation of frontal eye fields. *J Neurophysiol* 32: 637–648, 1969.

Schiller PH, True SD, Conway JL. Paired stimulation of the frontal eye fields and the superior colliculus of the rhesus monkey. *Brain Res* 179: 162–164, 1979.

Scudder CA, Moschovakis AK, Karabelas AB, Highstein SM. Anatomy and physiology of saccadic long-lead burst neurons recorded in the alert squirrel monkey. I. Descending projections from the mesencephalon. *J Neurophysiol* 76: 332–352, 1996.

Sommer MA, Wurtz RH. A pathway in primate brain for internal monitoring of movements. *Science* 296: 1480–1482, 2002.

Sommer MA, Wurtz RH. What the brain stem tells the frontal cortex. I. Oculomotor signals sent from superior colliculus to frontal eye field via mediodorsal thalamus. *J Neurophysiol* 91: 1381–1402, 2004.

Sooksawate T, Isa K, Behan M, Yanagawa Y, Isa T. Organization of GABAergic inhibition in the motor output layer of the superior colliculus. *Eur J Neurosci* 33: 421–432, 2011.

Sparks DL. Translation of sensory signals into commands for control of saccadic eye movements: role of primate superior colliculus. *Physiol Rev* 66: 118–171, 1986.

Sparks DL, Holland R, Guthrie BL. Size and distribution of movement fields in the monkey superior colliculus. *Brain Res* 113: 21–34, 1976.

Tehovnik EJ. Electrical stimulation of neural tissue to evoke behavioral responses. *J Neurosci Methods* 65: 1–17, 1996.

Van Gisbergen JA, Van Opstal AJ, Tax AA. Collicular ensemble coding of saccades based on vector summation. *Neuroscience* 21: 541–555, 1987.

Van Opstal A, Goossens H. Linear ensemble-coding in midbrain superior colliculus specifies the saccade kinematics. *Biol Cybern* 98: 561–577, 2008.

Van Opstal AJ, Kappen H. A two-dimensional ensemble coding model for spatial-temporal transformation of saccades in monkey superior colliculus. *Network* 4: 19–38, 1993.

Van Opstal AJ, Van Gisbergen JA. A nonlinear model for collicular spatial interactions underlying the metrical properties of electrically elicited saccades. *Biol Cybern* 60: 171–183, 1989.

Van Opstal AJ, Van Gisbergen JA. Role of monkey superior colliculus in saccade averaging. *Exp Brain Res* 79: 143–149, 1990.

Van Opstal AJ, Van Gisbergen JA, Smit AC. Comparison of saccades evoked by visual stimulation and collicular electrical stimulation in the alert monkey. *Exp Brain Res* 79: 299–312, 1990.

Vokoun CR, Jackson MB, Basso MA. Intralaminar and interlaminar activity within the rodent superior colliculus visualized with voltage imaging. *J Neurosci* 30: 10667–10682, 2010.

Walton MMG, Sparks DL, Gandhi NJ. Simulations of saccade curvature by models that place superior colliculus upstream from the local feedback loop. *J Neurophysiol* 93: 2354–2358, 2005.

Wilke M, Turchi J, Smith K, Mishkin M, Leopold DA. Pulvinar inactivation disrupts selection of movement plans. *J Neurosci* 30: 8650–8659, 2010.

Wurtz RH, Goldberg ME. Activity of superior colliculus in behaving monkey. III. Cells discharging before eye movements. *J Neurophysiol* 35: 575–586, 1972.